CHEMISTRY
A EUROPEAN JOURNAL

FULL PAPER

DOI: 10.1002/chem.201200292

Synthesis of Ni–Ru Alloy Nanoparticles and Their High Catalytic Activity in Dehydrogenation of Ammonia Borane

Guozhu Chen,*[a] Stefano Desinan,[a] Renzo Rosei,[b, c] Federico Rosei,[a, c, d] and Dongling Ma*[a]

Abstract: We report the synthesis and characterization of new Ni_xRu_{1-x} ($x = 0.56$–0.74) alloy nanoparticles (NPs) and their catalytic activity for hydrogen release in the ammonia borane hydrolysis process. The alloy NPs were obtained by wet-chemistry method using a rapid lithium triethylborohydride reduction of Ni^{2+} and Ru^{3+} precursors in oleylamine. The nature of each alloy sample was fully characterized by TEM, XRD, energy dispersive X-ray spectroscopy (EDX), and X-ray photoelectron spectroscopy (XPS). We found that the as-prepared Ni–Ru alloy NPs exhibited exceptional catalytic activity for the ammonia borane hydrolysis reaction for hydrogen release. All Ni–Ru alloy NPs, and in particular the $Ni_{0.74}Ru_{0.26}$ sample, outperform the activity of similar size monometallic Ni and Ru NPs, and even of Ni@Ru core-shell NPs. The hydrolysis activation energy for the $Ni_{0.74}Ru_{0.26}$ alloy catalyst was measured to be approximately 37 kJ mol^{-1}. This value is considerably lower than the values measured for monometallic Ni ($\approx$70 kJ mol^{-1}) and Ru NPs ($\approx$49 kJ mol^{-1}), and for Ni@Ru ($\approx$44 kJ mol^{-1}), and is also lower than the values of most noble-metal-containing bimetallic NPs reported in the literature. Thus, a remarkable improvement of catalytic activity of Ru in the dehydrogenation of ammonia borane was obtained by alloying Ru with a Ni, which is a relatively cheap metal.

Keywords: heterogeneous catalysis · hydrogen · hydrolysis · nickel · ruthenium

Introduction

Hydrogen is an environmentally friendly fuel and is regarded as one of the most promising future energy vectors.[1–3] Many key challenges, however, need to be addressed towards the transition to the so-called "hydrogen economy". The most prominent ones are: 1) finding new effective hydrogen-storage materials[4,5] and 2) efficient catalysts for the hydrogen-release reaction.[6,7] Recently, ammonia borane (NH_3–BN_3, AB for short) has been identified as one of the leading molecular candidates for hydrogen storage[8–11] because of its outstanding physicochemical properties, such as low molecular weight (30.87 g mol^{-1}), high (theoretical) stored hydrogen gravimetric capacity (19.6 wt%), high room-temperature stability in solid form (because of its polar nature and of intermolecular interactions between B and N atoms[8]), good stability in neutral and in alkaline aqueous solutions, safe and efficient release of hydrogen through either pyrolysis or hydrolysis routes. All of these features largely meet the US Department of Energy target for hydrogen on-board applications.[9]

The hydrolysis process is considered more promising, because it provides three mol of hydrogen per AB mol at room temperature in the presence of a suitable catalyst. Pyrolysis on the contrary is less appealing, because it releases only 6.5 wt% of hydrogen (i.e., $\approx$1 mol) and at a considerably higher temperature ($\approx$85 °C).[10] A number of different catalysts,[12–20] and in particular the noble metals (such as Pt,[18] Ru,[12,16,19] and Rh[20]), have been identified to be effective for accelerating AB hydrolysis. Their high price and limited abundance, however, hinder their practical application. Recently, a number of bimetallic catalysts based on much cheaper first-row transition metals have been reported to exhibit high efficiency for AB hydrolysis, even outperforming, in some cases, monometallic noble metals.[8,21–30] Sun and co-workers,[21] for example, found that $Co_{35}Pd_{65}$ NPs exhibited higher catalytic performance than monometallic Pd, and actually approached the activity of Pt NPs, which is considered a benchmark for AB hydrolysis. Yang

[a] Dr. G. Chen, Dr. S. Desinan, Prof. Dr. F. Rosei, Prof. Dr. D. Ma
Institut national de la recherché scientifique
1650, boulevard Lionel-Boulet, Varennes
Quebec, J3X 1S2 (Canada)
Fax: (+1) 514-875-8102
E-mail: ma@emt.inrs.ca
chen@emt.inrs.ca

[b] Prof. Dr. R. Rosei
Laboratorio "Nanotecnologie per l'Energia"
Consorzio per la Fisica
S.S. 14 Km 163.5, 34149 Trieste (Italy)

[c] Prof. Dr. R. Rosei, Prof. Dr. F. Rosei
Italy-Quebec Joint Laboratory in
Nanostructured Materials for Energy, Catalysis and
Biomedical Applications (Italy and Quebec)

[d] Prof. Dr. F. Rosei
Department Centre for Self-Assembled Chemical Structures
McGill University, Montreal, Quebec, H3A 2K6 (Canada)

Supporting information for this article is available on the WWW under http://dx.doi.org/10.1002/chem.201200292.

and co-workers[23] systematically compared a number of Ni- and Pt-based alloys and reported that most of these catalysts exhibited enhanced hydrogen-release rates with respect to either pure Pt or Ni metals. Xu and co-workers extensively studied bimetallic catalyst NPs for AB hydrolysis and found that Au@Co core-shell NPs,[26] Au–Ni embedded in SiO_2,[27] Fe–Ni alloy,[28] and Cu@M (M = Co, Fe, Ni) core-shell NPs[29] exhibited a markedly higher catalytic activity than their monometallic counterparts. All the above results indicate that formation of certain bimetallic NPs could increase the catalyst efficiency in the hydrolysis of AB, and at the same time, it could dramatically lower the cost of the catalysts by decreasing the consumption of noble metals.

Ru is one of the most widely studied catalysts for AB dehydrogenation. It is therefore promising to try to improve its activity and simultaneously minimize its use by forming Ru-based bimetallic structures. Recently, bimetallic Ru–Co and Ru–Cu catalysts supported on Al_2O_3 were synthesized by a polyol method, and their activities for AB dehydrogenation were evaluated. It was found that alloying these metals with Ru, especially in the case of Ru–Co (1:1), induces a clear catalytic activity increase with respect to monometallic Ru. However, NPs and large aggregates were present together, and the structure (alloy or core shell) of these bimetallic compounds could not be easily determined.[31] Most recently, our group reported the synthesis of monodisperse Ni@Ru core-shell NPs, showing that this material has good catalytic performance for AB hydrolysis.[32] We attributed their high activity to the ultrasmall size of the Ru NPs and the interfacial interaction between Ni-core and Ru-shell atoms. Investigating the catalytic activity of other Ni–Ru bimetallic arrangements with different geometries and different compositions looks attractive therefore, because it may offer the possibility of fine tuning their catalytic activity towards faster hydrogen release in the AB hydrolysis reaction.

It is known that the Ni and Ru are essentially immiscible at equilibrium because of their positive enthalpy of formation.[33] It is not easy to synthesize Ni–Ru alloys at ordinary temperatures and mild conditions. Recently, El-Gendy et al. successfully synthesized carbon-coated Ni–Ru alloy NPs at 900 °C by high-pressure chemical-vapor deposition by using metallocenes as metal precursors.[34] The impregnation method was also employed to synthesize bimetallic Ni–Ru NPs supported on graphite and SBA-15 silica.[35,36] However, the impregnation method is not conducive for controlling particle size and compositional homogeneity.

In this work, nearly monodisperse Ni–Ru alloy NPs were synthesized by using a colloidal synthetic approach, and the evaluation of catalytic activity towards hydrolysis of AB was carried out. TEM images show that over all different compositions, the resulting NPs have similar size ($\approx$9 nm) and similar size distributions. EDX, XPS, and STEM show in all cases a homogeneous (at the nanometer scale) Ni/Ru atomic-ratio distribution across the NPs. XRD data reveal that the NPs have all-crystalline face-centered cubic (fcc) structure, and that the lattice parameter increases with the Ru/Ni concentration ratio. Interestingly, catalytic evaluation demonstrates the Ni–Ru alloy NPs have remarkable activity compared with monometallic NP components and Ni@Ru core-shell NPs, and also outperform most noble-metal-containing bimetallic NPs reported.

Results and Discussion

Recently, various metals immiscible in bulk form (such as Au–Pt,[37] and Ag–Rh[38]) were successfully alloyed at the nanometer size by using wet-chemistry methods. This is possible, because at the nanoscale, alloy-formation enthalpies may become negative in some cases.[39] In the case of the Ni–Ru system, the two elements have a large standard reduction-potentials difference, and a fast reduction process is required for trapping Ni and Ru into an alloy, thus avoiding separate nucleation. In this study, a strong reducing agent, a preheated precursor solution and a high-boiling solvent proved effective for this purpose.[37,40] Accordingly, Ni–Ru alloy NPs were prepared by using a hot-injection method with co-reduction of $Ni(acac)_2$ and $[Ru(acac)_3]$ (acac = acetylacetonate) in oleylamine by using superhydride ($LiBEt_3H$) as the reducing agent. Note that if a weaker reducing agent (such as $NaBH_4$) is employed instead, separate nucleation of Ni and Ru NPs occurs as shown in Figure S1 in the Supporting Information. Oleylamine and oleic acid were employed as capping agents to control the particle size and shape. With this procedure, we obtained Ni–Ru alloy NPs with several different compositions. The compositions of the as-prepared alloy NPs were investigated by neutron activation analysis (NAA). The discrepancy between Ni/Ru atomic ratios in precursors and in the NPs may result from the kinetic difference in the reduction of the Ru—oleic-acid complex with respect to Ni–oleic acid, even though ruthenium ions are more easily reduced than nickel ions according to their reduction potentials.[41] XRD patterns of as-prepared alloy NPs with different Ni/Ru concentration ratio, along with those of pure Ni and Ru NPs, are displayed in Figure 1.

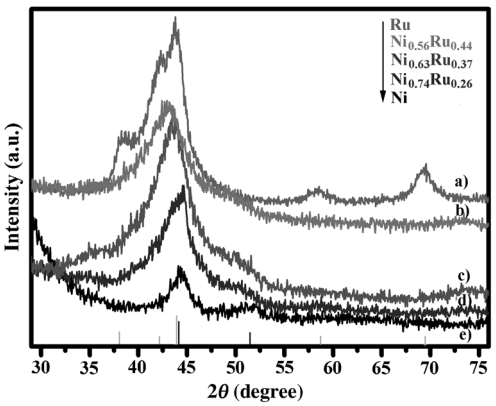

Figure 1. XRD patterns of pure a) Ru, b) $Ni_{0.56}Ru_{0.44}$, c) $Ni_{0.63}Ru_{0.37}$, d) $Ni_{0.74}Ru_{0.26}$, and e) pure Ni. Gray vertical lines represent the hcp Ru phase (JCPDS file 06-0663) and black vertical lines the fcc Ni phase (JCPDS file 04-0850).

It can be seen that the XRD pattern of pure Ni NPs matches that of fcc-structured Ni (JCPDS file 04-0850), and the XRD pattern of pure Ru NPs corresponds to that of hexagonal close-packed (hcp)-structured Ru (JCPDS file 06-0663). All the alloy samples exhibit fcc structure reflections, indicating the formation of fcc metallic alloys. Moreover, the diffraction peaks shifted to lower angles as the atomic percentage of Ru increased, demonstrating a lattice expansion originating from the substitution of the larger Ru atoms in place of the smaller Ni atoms.

Figure 2a shows a representative TEM image of a $Ni_{0.74}Ru_{0.26}$ NPs sample, showing rounded particles with approximately 9 nm average diameter. Similar morphologies

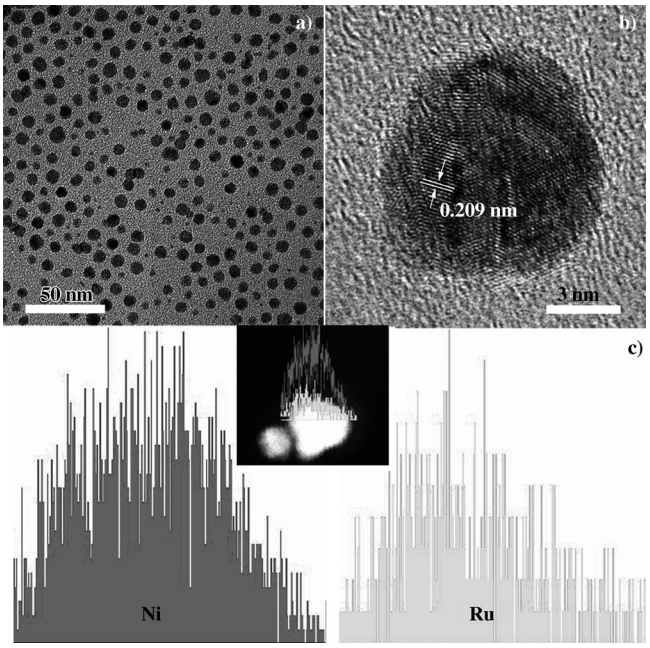

Figure 2. a) TEM image of a $Ni_{0.74}Ru_{0.26}$ alloy NPs sample; b) HRTEM image of a single $Ni_{0.74}Ru_{0.26}$ alloy NP; c) Ni and Ru compositional-line profiles recorded along the median line of a single particle in the STEM image (see inset).

and sizes were observed for the $Ni_{0.63}Ru_{0.37}$ and $Ni_{0.56}Ru_{0.44}$ NPs. In contrast, the size of pure Ru NPs synthesized by using the same superhydride reduction method is only 3–4 nm (Figure S2 in the Supporting Information). Selected area electron diffraction (SAED) pattern of these Ni–Ru alloy NPs exhibits diffraction rings with fcc features (Figure S3 in the Supporting Information), confirming XRD findings. Figure 2b shows a typical HRTEM image of a single $Ni_{0.74}Ru_{0.26}$ NP, in which lattice fringes can be clearly observed throughout the whole particle, demonstrating the crystalline nature of our NPs. The fringes showed an average lattice separation of 0.209 nm, which differs from both the Ru {100} crystal plane (0.238 nm) and the Ni {111} plane (0.206 nm). Although Ru NPs are monocrystalline, and pure Ni NPs are either monocrystalline or twinned (Figure S4 in the Supporting Information), alloy nanoparticles are polycrystalline. TEM–EDS point spectra acquired from different individual $Ni_{0.74}Ru_{0.26}$ NPs show the coexistence of both metals in every tested single NP (Figure S5 in the Supporting Information). To further investigate the distribution of Ni and Ru atoms within an individual NP, a single NP was linearly scanned by using a 2 nm EDS probe in a JEOL 2100 TEM operating in the STEM mode. As can be seen in Figure 2c, both elements show the similar Gaussian distribution across the NP, further indicating that it has a random homogeneous (at the nanometer scale) alloy structure.

XPS was used to detect catalyst samples' surface composition and to provide further proof of alloy structure homogeneity by using progressive sample etching.[26] As shown in Figure 3, the appearance of the characteristic peaks for met-

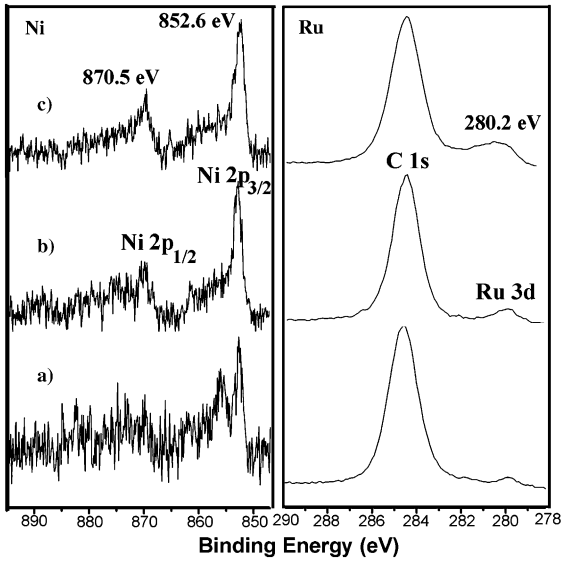

Figure 3. Left panel: Ni XPS spectra of the $Ni_{0.74}Ru_{0.26}$ alloy NPs: a) before Ar^+ ion sputter etching; b) after 2 min etching; c) after 5 min etching. Right panel: Ru XPS spectra of the $Ni_{0.74}Ru_{0.26}$ alloy NPs in the same conditions as reported in the left panel.

allic Ni 2p and Ru 3d in the XPS spectra indicates the coexistence of both elements in the Ni–Ru NPs. Owing to the surface-ligands coverage, the intensities of Ni and Ru are both weak (Figure 3a). They increase simultaneously and markedly after 2 and 5 min etching. This trend is different from that of Ni@Ru core-shell NPs,[32] in which the Ni/Ru spectra–intensity ratio increases with the etching depth. Here, the Ni/Ru intensity ratio remains almost the same, demonstrating similar Ni/Ru ratio between the surface and inner part in the as-prepared Ni-Ru alloy NPs.

To study NPs catalysis, all our samples were first loaded onto high specific-surface area carbon black (CB) and then dispersed in water. The TEM image of the Ni–Ru alloy NPs/CB catalyst (Figure S6 in the Supporting Information) shows that NPs preserve their size and shape after dispersion onto the carbon support. The activity of Ni–Ru alloy NPs with different compositions were evaluated for the AB

dehydrogenation reaction, and the results were compared to the activity of similar size monometallic Ni, Ru, and Ni@Ru core-shell NPs (Figure S7 in the Supporting Information). Because NPs with different size and surface ligands exhibit significant differences in catalytic activity, to guarantee a fair comparison, monometallic Ru NPs prepared from $[Ru_3(CO)_{12}]$ decomposition in oleylamine were used (instead of the $Ru(acac)_3$ derived), because they have a size close to that of Ni–Ru alloy NPs. Figure 4 shows hydrogen

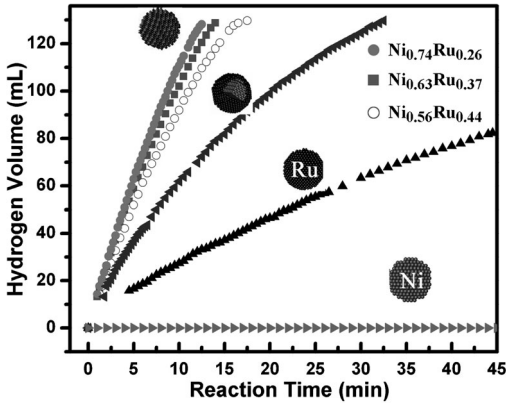

Figure 4. Comparison of catalytic activities of monometallic Ni, monometallic Ru, Ni@Ru core shell, and Ni–Ru alloy NPs for AB hydrolysis at 30±1°C. [Ru]=0.25 mM in monometallic Ru, in Ni@Ru, and in Ni–Ru alloy NPs; for monometallic Ni, [Ni]=1 mM; [AB]: 200 mM; volume of the dispersion=10 mL.

evolution curves during the AB hydrolysis reaction. All bimetallic NPs catalysts were normalized with respect to the weight of active Ru, because Ru is the more expensive component of our NPs (the price of Ru is close to that of Pt and Au). It is evident that Ru NPs/CB exhibited certain activity in this reaction, whereas monometallic Ni NPs/CB exhibited almost no catalytic activity towards the hydrolysis of AB within 45 min at 30°C, even at a concentration four times higher than that of Ru. Impressively, the hydrogen release in the presence of bimetallic Ni–Ru NPs/CB is significantly accelerated with respect to both Ru NPs/CB and Ni NPs/CB. Such improvement of the catalytic activity of Ni–Ru bimetallic NPs in comparison with monometallic Ru NPs indicates an effect that goes well beyond the simple physical addition of Ni. In addition, all Ni–Ru alloy NPs presented higher activity than our previously measured Ni@Ru core-shell NPs. Specifically, the dehydrogenation reaction of AB is complete within 12 min for $Ni_{0.74}Ru_{0.26}$ NPs; in contrast, it takes almost three times as long in the presence of Ni@Ru core-shell NPs.

We repeated the activity measurements for AB hydrolysis for a selected number of samples, to evaluate their apparent activation energy barrier for the AB hydrolysis reaction. Figure 5 shows the hydrogen-generation rates of $Ni_{0.74}Ru_{0.26}$, of monometallic Ru and of Ni@Ru core-shell NPs at different temperatures in the range of 20–60°C. The apparent ac-

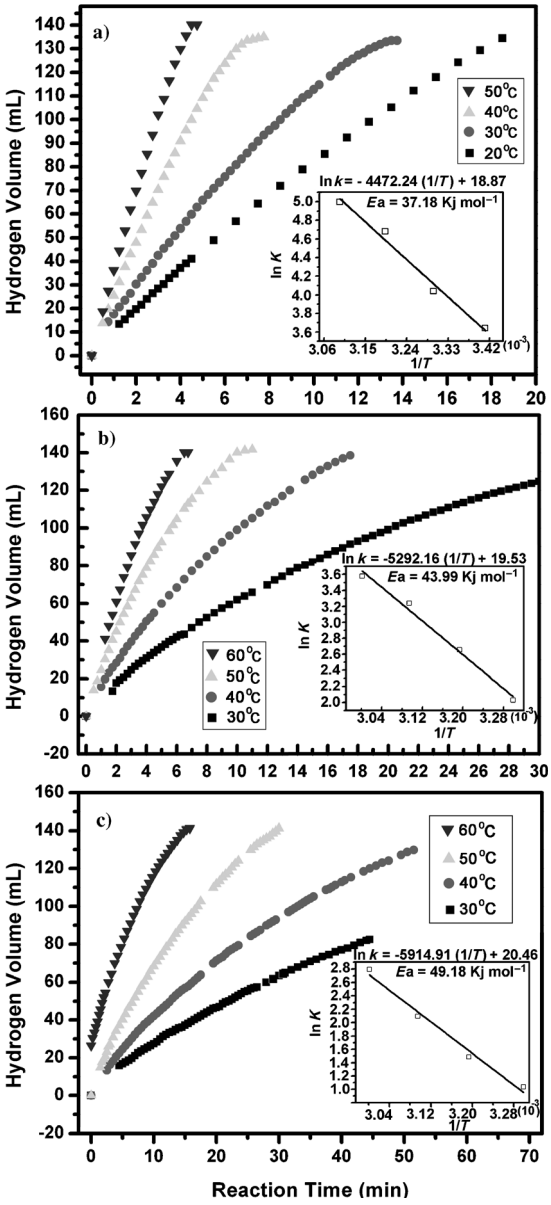

Figure 5. Plots of hydrogen production versus time during AB hydrolysis at different temperatures for a) $Ni_{0.74}Ru_{0.26}$ alloy NPs; b) Ni@Ru core-shell NPs; c) monometallic Ru NPs. Insets show the reaction's Arrhenius plot in each case.

tivation energies were determined to be approximately 37.18 kJ mol^{-1} for the Ni–Ru alloy, about 43.99 kJ mol^{-1} for the Ni@Ru core-shell, and about 49.18 kJ mol^{-1} for the monometallic Ru catalysts. The activation energy of monometallic Ni NPs was also measured and found to be about 70.31 kJ mol^{-1} (Figure S8 in the Supporting Information). The Ni–Ru alloy NPs present the lowest activation barrier among the catalysts we have tested, and it is also smaller than the activation energies reported for most Ru-based catalysts (Ru, RuCo, and RuCu bimetallic catalysts[12,16,19,31]). Furthermore, it is also smaller than that of other noble-metal monometallic catalysts, such as Pd[42,43] and Rh.[20]

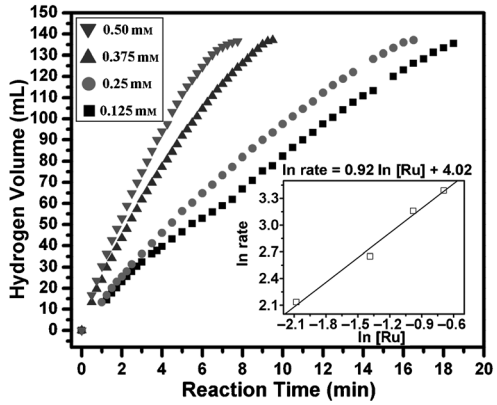

Figure 6. Plots of hydrogen evolution versus time during AB hydrolysis catalyzed by $Ni_{0.74}Ru_{0.26}$ NPs at 30 ± 1 °C and at different catalyst concentrations. The inset shows the plot of hydrogen-generation rate versus catalyst concentration (both in logarithmic scales).

Figure 6 shows the plot of the H_2 gaseous volume generated from the hydrolysis of AB solution in the presence of different $Ni_{0.74}Ru_{0.26}$ NPs concentrations at 30 ± 1 °C. The inset shows the plot of the hydrogen-evolution rate versus catalyst concentration in a log–log scale. The line slope is 0.92, indicating that the hydrolysis reaction is essentially first order with respect to catalyst concentration. A reusability test showed that the $Ni_{0.74}Ru_{0.26}$ NPs still exhibited high catalytic activity after five cycles of reaction (Figure S9 in the Supporting Information).

In the hydrolysis process, an AB molecule first diffuses onto the catalyst surface and forms an activated complex, which dissociates upon attack of a water molecule, liberating H_2.[43,44] Catalytic properties are closely correlated with the catalyst surface geometric and electronic structures, and an optimal compromise among reactant adsorption rate, adsorbate–surface interaction and product desorption promotes catalytic activity.[45] The results we obtained are very interesting yet not straightforward to explain. In essence, we found that we can obtain a much better catalyst for the AB hydrogenation reaction by alloying Ni (which is not active for the reaction yet relatively cheap), with Ru (which is only mildly active). A comparison with literature[18,21] shows that our catalyst activity is close to the activity of Pt. Both these findings are difficult to reconcile with the NPs' surface structure, in which Ni and Ru are randomly interspersed (because in this case the reactivity should have an intermediate value between Ni and Ru, which is obviously not the case). Tentatively, our results could be explained by a surface structure, in which Ru atoms form small (monolayer) islands surrounded by Ni atoms. This is plausible, because Ru–Ru bonds are stronger than Ru–Ni bonds, and NPs' surface atoms are relatively mobile even at low temperature.[46] According to the d-band model, the activity of Ru islands' atoms (which sit mostly on second-layer Ni atoms), would be lowered by a synergistic combination of strain (because Ru atomic radius is larger than the radius of Ni) and ligand effects. The concerted action of these two effects would lower the projected center of the d band (with respect to the Fermi surface), thus lowering the local chemical reactivity (to values close to Pt's).[47]

Conclusion

In summary, we synthesized Ni–Ru alloy NPs with different Ni/Ru ratios by a simultaneous reduction method, and we characterized them extensively. XRD and SAED patterns display an fcc structure for all the as-prepared Ni–Ru alloys. The coexistence and homogeneous distribution of Ru and Ni within an individual NP was further confirmed by STEM–EDS line profiles. Our AB hydrolysis kinetic data demonstrate that alloying with Ni decreases the apparent reaction activation energy, significantly enhancing the catalytic activity of Ru. The order of the reaction with respect to the catalyst concentration is about one, that is, the same as that had been reported for monometallic Ru. $Ni_{0.74}Ru_{0.26}$ NPs (the most Ni-rich alloy among the NP alloys tested in this work) presented the highest catalytic activity for the AB hydrolysis reaction. Ni–Ru alloy NPs represents an improvement also in comparison with the previously studied Ni@Ru NPs in the core-shell arrangement. The relative preparation simplicity of these new catalysts and the relatively low Ru content make Ni–Ru alloys realistic candidates for practical applications. This result further demonstrates that the catalytic activity can be tuned by forming appropriate bimetallic structures. In particular, we showed that bimetallic alloy NPs can be synthesized with chemical reactivity mimicking those of noble metals. This may allow in the future either to replace, or at least reduce, the amount of noble metals in catalyst formulation. The Ni–Ru alloys may also exhibit improved catalytic activity in other heterogeneous catalysis reactions (e.g., hydrogenation of acetonitrile[35]), in which Ni and/or Ru are involved.

Experimental Section

Synthesis of Ni–Ru alloy NPs: All chemicals used were purchased from Sigma–Aldrich. Electro-conductive CB Ketjenblack EC-300 J was obtained from AkzoNobel. All syntheses were carried out by using standard airless procedures with Ar flow as inert gas. The synthesis method was similar to that used by Yang et al. for Pt–Ni NPs.[40] In a typical synthesis of $Ni_{0.74}Ru_{0.26}$ NPs, nickel(II) acetylacetonate (64 mg) was dissolved in diphenyl ether (5 mL) containing oleic acid (0.75 mL). The solution was heated to about 120 °C and kept at this temperature for 20 min to remove humidity and oxygen. Next, the solution was cooled to about 90 °C, and ruthenium(III) acetylacetonate (33.2 mg) and Super-Hydride® solution (1 mL, 1.0 M lithium triethylborohydride in THF) was quickly injected into the solution. After 1 min, the as-prepared mixture was transferred into a flask containing oleylamine (15 mL), which had been preheated to about 300 °C. The mixture was kept at 250 °C for 15 min and then cooled to RT. Ethanol (60 mL) was added to precipitate the NPs, and the product was collected by centrifugation at 9000 rpm for 10 min. The obtained NPs were further washed twice in ethanol and then dispersed in hexane. By changing the precursor ratio between nickel(II) acetylacetonate and ruthenium(III) acetylacetonate, the alloy NPs of different compositions were prepared, with nominal Ni/Ru ratios 3:1, 1:1, and

1:3, which respectively led to catalysts with $Ni_{0.74}Ru_{0.26}$, $Ni_{0.63}Ru_{0.37}$ and $Ni_{0.56}Ru_{0.44}$ compositions. The final composition of the alloy NPs was obtained from NAA. Monometallic Ni, Ru, and Ni@Ru core-shell NPs were synthesized according to previously reported methods.[32]

Characterization: To prepare the samples for XRD and XPS measurements, Si wafers were washed thoroughly with acetone and ethanol for three times. After dropping the NPs dispersing in hexane on the cleaned Si wafer, they were dried at RT. The as-prepared samples were analyzed by XRD at grazing-angle incidence (X-Pert Pro (PANalytical) Diffractometer). The angle between sample surface and incident beam was fixed at 3°. The experimental resolution and the integration time per step were 0.05° and 4 s, respectively. XPS was taken by using a VG Escalab 220i-XL equipped with a twin-anode (Mg/Al) source. The etching was carried out by Ar sputtering under the conditions of a background vacuum of 2.0×10^{-8} mbar, a sputtering acceleration voltage of 3.0 kV, and a sputtering current of 100 nA. To correct for charging, the binding energies (BE) were referred to the C1s peak at 284.6 eV. TEM (JEOL 2100F) and EDX were applied for a detailed analysis of microstructure and composition. The samples for TEM, SAED, and EDS were prepared by depositing one or two droplets of the NPs colloidal suspension in hexane onto copper grids coated with a thin carbon film. NAA (SLOWPOKE) was conducted to analyze the amounts of Ni and Ru in the prepared Ni–Ru alloy, monometallic Ni and Ru, and Ni@Ru core-shell NP dispersions.

AB catalytic hydrolysis tests: The Ketjenblack CB was dispersed in the colloidal dispersion of NPs in hexane, and this mixture was stirred until the hexane was completely evaporated. Water was then added to the NPs/CB. Because the NPs and carbon are both hydrophobic, ultrasonication was required to obtain a uniform dispersion. To start the reaction, AB water solution (63 mg) was introduced into the aqueous dispersion of NPs/CB catalysts under vigorous stirring. The data we report on performance comparison and durability, refer to catalysts that were used once in a preliminary catalytic run, then washed and re-dispersed in water. The volume of evolved hydrogen gas was measured by recording the displacement of water level in an inverted and graduated water-filled burette (Aldrich® graduated burette). The hydrogen-generation rate at different concentrations and the values of the rate constant k at different temperatures were calculated from the initial slope of the H_2 release versus time for each experiment.

Acknowledgements

Financial support from the Natural Sciences and Engineering Research Council of Canada (NSERC) through a Strategic Grant, and Agence de l'efficacité énergétique is greatly appreciated. F.R. is grateful to MDEIE and to MAE (Italy) for partial funding of the Italy–Quebec Joint Laboratory in Nanostructured Materials for Energy, Catalysis, and Biomedical Applications. R.R. is grateful to EOARD for partial funding of the project.

[1] Z. Xiong, C. K. Yong, G. Wu, P. Chen, W. Shaw, A. Karkamkar, T. Autrey, M. O. Jones, S. R. Johnson, P. P. Edwards, W. I. F. David, *Nat. Mater.* **2008**, *7*, 138.
[2] T. Hügle, M. Hartl, D. Lentz, *Chem. Eur. J.* **2011**, *17*, 10184.
[3] H.-L. Jiang, Q. Xu, *Catal. Today* **2011**, *170*, 56.
[4] T. Hügle, M. F. Kühnel, D. Lentz, *J. Am. Chem. Soc.* **2009**, *131*, 7444.
[5] P. Jena, *J. Phys. Chem. Lett.* **2011**, *2*, 206.
[6] T. He, Z. Xiong, G. Wu, H. Chu, C. Wu, T. Zhang, P. Chen, *Chem. Mater.* **2009**, *21*, 2315.
[7] Ö. Metin, S. Özkar, *Energy & Fuels* **2009**, *23*, 3517; Fuels **2009**, 23, 3517.
[8] Y. Li, L. Xie, Y. Li, J. Zheng, X. Li, *Chem. Eur. J.* **2009**, *15*, 8951.
[9] Y. Guo, X. He, Z. Li, Z. Zou, *Inorg. Chem.* **2010**, *49*, 3419.
[10] A. Staubitz, A. P. M. Robertson, I. Manners, *Chem. Rev.* **2010**, *110*, 4079.
[11] Y. S. Chua, G. Wu, Z. Xiong, T. He, P. Chen, *Chem. Mater.* **2009**, *21*, 4899.
[12] F. Durap, M. Zahmakıran, S. Özkar, *Int. J. Hydrogen Energy* **2009**, *34*, 7223.
[13] J.-M. Yan, X.-B. Zhang, H. Shioyama, Q. Xu, *J. Power Sources* **2010**, *195*, 1091.
[14] Ö. Metin, V. Mazumder, S. Özkar, S. Sun, *J. Am. Chem. Soc.* **2010**, *132*, 1468.
[15] M. Fetz, R. Gerber, O. Blacque, C. M. Frech, *Chem. Eur. J.* **2011**, *17*, 4732.
[16] S. Basu, Y. Zheng, A. Varma, W. N. Delgass, J. P. Gore, *J. Power Sources* **2010**, *195*, 1957.
[17] Ö. Metin, S. Duman, M. Dinç, S. Özkar, *J. Phys. Chem. C* **2011**, *115*, 10736.
[18] X. Yang, F. Cheng, Z. Tao, J. Chen, *J. Power Sources* **2011**, *196*, 2785.
[19] Ö. Metin, S. Sahin, S. Özkar, *Int. J. Hydrogen Energy* **2009**, *34*, 6304.
[20] S. Karahan, M. Zahmakıran, S. Özkar, *Int. J. Hydrogen Energy* **2011**, *36*, 4958.
[21] D. Sun, V. Mazumder, Ö. Metin, S. Sun, *ACS Nano* **2011**, *5*, 6458.
[22] W. H. Shin, H. M. Jung, Y. J. Choi, K. Miyasaka, J. K. Kang, *J. Mater. Chem.* **2010**, *20*, 6544.
[23] C. F. Yao, L. Zhuang, Y. L. Cao, X. P. Ai, H. X. Yang, *Int. J. Hydrogen Energy* **2008**, *33*, 2462.
[24] X. Yang, F. Cheng, J. Liang, Z. Tao, J. Chen, *Int. J. Hydrogen Energy* **2011**, *36*, 1984.
[25] F. Cheng, H. Ma, Y. Li, J. Chen, *Inorg. Chem.* **2007**, *46*, 788.
[26] J.-M. Yan, X.-B. Zhang, T. Akita, M. Haruta, Q. Xu, *J. Am. Chem. Soc.* **2010**, *132*, 5326.
[27] H.-L. Jiang, T. Umegaki, T. Akita, X.-B. Zhang, M. Haruta, Q. Xu, *Chem. Eur. J.* **2010**, *16*, 3132.
[28] J.-M. Yan, X.-B. Zhang, S. Han, H. Shioyama, Q. Xu, *J. Power Sources* **2009**, *194*, 478.
[29] H.-L. Jiang, T. Akita, Q. Xu, *Chem. Commun.* **2011**, *47*, 10999.
[30] S. K. Singh, Y. Lizuka, Q. Xu, *Int. J. Hydrogen Energy* **2011**, *36*, 11794.
[31] G. P. Rachiero, U. B. Demirci, P. Miele, *Int. J. Hydrogen Energy* **2011**, *36*, 7051.
[32] G. Chen, S. Desinan, R. Nechache, R. Rosei, F. Rosei, D. Ma, *Chem. Commun.* **2011**, *47*, 6308.
[33] X. He, L. T. Kong, J. H. Li, X. Y. Li, B. X. Liu, *Acta Mater.* **2006**, *54*, 3375.
[34] A. A. El-Gendy, V. O. Khavrus, S. Hampel, A. Leonhardt, B. Büchner, R. Klingeler, *J. Phys. Chem. C* **2010**, *114*, 10745.
[35] P. Braos-García, C. García-Sancho, A. Infantes-Molina, E. Rodríguez-Castellón, A. Jiménez-López, *Appl. Catal. A* **2010**, *381*, 132.
[36] M. Cerro-Alarcón, A. Maroto-Valiente, I. Rodríguez-Ramos, A. Guerrero-Ruiz, *Appl. Catal. A* **2004**, *275*, 257.
[37] S. Zhou, G. S. Jackson, B. Eichhorn, *Adv. Funct. Mater.* **2007**, *17*, 3099.
[38] J. Kim, Y. Lee, S. Sun, *J. Am. Chem. Soc.* **2010**, *132*, 4996.
[39] S. Xiong, W. Qi, B. Huang, M. Wang, *ChemPhysChem* **2011**, *12*, 1317.
[40] H. Yang, J. Zhang, S. Kumar, H. Zhang, R. Yang, J. Fang, S. Zou, *Electrochem. Commun.* **2009**, *11*, 2278.
[41] S. K. Son, Y. Jang, J. Park, H. B. Na, H. M. Park, H. J. Yun, J. Lee, T. Hyeon, *J. Am. Chem. Soc.* **2004**, *126*, 5026.
[42] M. Rakap, S. Özkar, *Int. J. Hydrogen Energy* **2011**, *36*, 7019.
[43] M. Rakap, S. Özkar, *Int. J. Hydrogen Energy* **2010**, *35*, 1305.
[44] Q. Xu, M. Chandra, *J. Power Sources* **2006**, *163*, 364.
[45] J. K. Nørskov, T. Bligaard, A. Logadottir, S. Bahn, L. B. Hansen, M. Bollinger, H. Bengaard, B. Hammer, Z. Sljivancanin, M. Mavrikakis, Y. Xu, S. Dahl, C. J. H. Jacobsen, *J. Catal.* **2002**, *209*, 275.
[46] L.-L. Wang, D. D. Johnson, *J. Am. Chem. Soc.* **2009**, *131*, 14023.
[47] A. Groß, *J. Phys. Condens. Matter* **2009**, *21*, 084205.

Received: January 27, 2012
Revised: March 22, 2012
Published online: April 26, 2012

